Yb^{3+} doping effects on thermal conductivity and thermal expansion of Yttrium aluminium garnet

Jing Wang[1], Fang Xu[1], R. J. Wheatley[2], Nigel Neate[1], Xianghui Hou[1*]

[1]*Department of Mechanical, Materials and Manufacturing Engineering, Faculty of Engineering, University of Nottingham, Nottingham, NG7 2RD, UK*

[2] *School of Chemistry, University of Nottingham, Nottingham, NG7 2RD, UK*

Abstract

Yttrium Aluminium Garnet (YAG) is an attractive candidate as thermal barrier material used for turbine blade in aero engines, due to its relatively low thermal conductivity, low oxygen diffusivity and good phase stability at high temperature. YAG has a complex crystal structure, in which Y^{3+} ions locate in dodecahedron and Al^{3+} ions in octahedron and tetrahedron. Replacing the host cations with rare earth elements can cause the structure change which influences the thermal properties of YAG. Because the space inside the octahedron is relatively small, Yb^{3+} ions which have the smallest ionic radial size in the lanthanide series, have been selected and attempted to be doped on dodecahedral and octahedral sites to investigate the effects on thermal conductivity and thermal expansion. The variation of lattice constant indicates that Yb^{3+} ions are located on the dodecahedron or octahedron. In addition, when Yb^{3+} ions replace Al^{3+} ions on octahedral sites, the thermal conductivity at room temperature is dramatically reduced and the coefficient of thermal expansion is over 10×10^{-6} K^{-1} at high temperature, which results from the expansion of octahedron due to the much larger radius of Yb^{3+} ion compared with the host cation (Al^{3+} ion). On the contrary, replacing Y^{3+} ions with Yb^{3+} ions in dodecahedron, the thermal conductivity also gradually reduces to the similar value but the coefficient of thermal expansion is getting smaller, due to the

relatively smaller ionic radius of Yb^{3+} causing the contraction of the dodecahedron. Therefore, a dopant with much larger radius would be preferred in both dodecahedron and octahedron to significant reduce thermal conductivity as well as increase coefficient of thermal expansion of YAG, by introducing large radial difference between the dopant and the host cations.

Keywords: Thermal Barrier Coating; Yttrium Aluminium Garnet; Thermal Conductivity; Coefficient of Thermal Expansion.

*Corresponding Author, email: xianghui.hou@nottingham.ac.uk

Tel: +44 115 95 13920, Fax: +44 115 95 13800

1 Introduction

Thermal barrier coatings (TBCs) with low thermal conductivity and high coefficient of thermal expansion have attracted increasing interest to avoid the melting and oxidation of metal alloy components in gas turbine. One of the most important factors responsible for TBC failure is the oxidation of the metal bond coat [1], which results in the formation of a oxide grown layer (TGO) sandwiched between the metal substrate and the conventional yttria stabilized zirconia coating [2, 3]. The oxygen contributed to the TGO formation usually comes from two sources: one source is from the engine combustion environment, where oxygen can transport through the zirconia coating along the micro-cracks or pores in the coating; another source is from zirconia coating, in which oxygen atom can diffuse through oxygen vacancies within zirconia [4]. The oxygen diffusivity is a dominant factor for determining the thickness of TGO that is closely related to the life time of TBCs. In addition, a new material with good phase stability is desired to be used at high operating temperature, *e.g.* 1400^{o}C, due to the poor phase stability of the conventional yttira stabilized zirconia (7~8YSZ) at high temperature (above 1250^{o}C). And also, the coefficient of thermal expansion between top ceramic coating and metal alloy are quite different, which is easy to generate stress between the layers due to the expansion mismatch, thus it is also very important to increase the thermal expansion of ceramic top coat materials.

Yttrium aluminium garnet $Y_3Al(1)_2Al(2)_3O_{12}$ ($A_3B_2C_3O_{12}$, YAG) has excellent phase/thermal stability up to the melting point (1970^{o}C), and its oxygen diffusivity is about 10 orders of magnitude lower than that in zirconia. It offers a promising alternative to conventional zirconia to improve life time of TBCs [5-9]. YAG has the relatively high thermal conductivity, 3.2 W·m·K^{-1} [10] and low coefficient of thermal expansion, ~8×10^{-6} K^{-1} [11], if compared with the values of 7~8YSZ (1.35 W·m·K^{-1} for thermal conductivity, and ~10×10^{-6}

K^{-1} for coefficient of thermal expansion) [12]. So far, the study of YGA for TBC application is mainly based on un-doped YAG, to construct TBC bilayer consisting of porous YSZ with YAG top layer [7, 13, 14]. Liu *et al* found that Er doped YAG on dodecahedral site can reduce thermal conductivity, but also decrease coefficient of thermal expansion [15]. From **Figure 8(a),** it can be seen that YAG has three polyhedrons in a unit cell, including Y^{3+} ions locating in dodecahedron (A site), and Al^{3+} ions in octahedron (B site) and tetrahedron (C site) in the ratio of 2:3, where three dodecahedrons share their edges to each other and share the edges with three octahedrons shown in **Figure 8 (b)**. The doping and doping position would have great influences on the crystal structure and thermal properties. But there is no report that studies how doping mechanism would affect thermal properties by substituting the atoms in dodecahedron or octahedron.

The purpose of this work is to investigate the doping effects of dodecahedron and octahedron on thermal conductivity and thermal expansion of YAG. Because the space inside the octahedron is relatively small, Yb^{3+} ions which have the smallest ionic radial size in the lanthanide series, have been selected to be doped on dodecahedral and octahedral sites to investigate the effects on thermal conductivity and thermal expansion. In YAG, if the doping site is different, the ionic radius of Yb^{3+} changes with the numbers of neighbouring oxygens, named coordination numbers. When the coordination number is 8 for the dodecahedron, Yb^{3+} with ionic radius of 0.985 Å is to replace Y^{3+} ion with the relatively large ionic radius of 1.019 Å[16, 17]. For the octahedron, the coordination number is 6, so Yb^{3+} with much larger ionic radius (0.868 Å) is to replace the Al^{3+} ion (0.535 Å) [18, 19]. Therefore, it is expected that this radial difference will significantly influence thermal conductivity and thermal expansion by causing the distortion of polyhedron.

2 Experimental work

2.1 Preparation of ceramic powders

Sol-gel method was selected to synthesize un-doped Yttrium aluminium garnet (YAG, $Y_3Al_5O_{12}$) and Yb doped YAG [$(Yb_xY_{1-x})_3Al_2Al_3O_{12}$ where, x=0.05, 0.15, and 0.2 and, $Y_3(Yb_xAl_{1-x})_2Al_3O_{12}$ where x= 0.005, 0.015 and 0.02] Ytterbium nitrate pentahydrate (Sigma-Aldrich, 99.9%), yttrium nitrate hexahydrate (Sigma-Aldrich, 99.8%) and aluminium nitrate nonahydrate (Sigma- Aldrich, 98%) were chosen as raw materials and citric acid (Sigma-Aldrich, 99%) as organic complexing agent. Methanol (Sigma- Aldrich, 8%) was chosen as solvent. Firstly, certain amount of raw materials determined by stoichiometry of each composition was dissolved in methanol. The doping mole ratio of Yb/Y or Yb/Al and the descriptions of the compositions are given in **Table 1**. Then ytterbium nitrate pentahydrate and yttrium nitrate hexahydrate solutions were slowly dropped into aluminium nitrate nonahydrate solution under magnetic stirring at room temperature. After stirring for 30 min, citric acid solution was dropped, where a molar ratio of citric acid/cation ions is 1.2/1.0. The forerunner was stirred for 3 h at room temperature. Then the mixed solution was moved into a furnace at 80^{o}C until the dried gel was obtained. The dried gel was placed into alumina crucible and heat-treated at 500^{o}C by 2 ^{o}C/min for 4 h to remove carbon from organic components, then heating up to 950^{o}C with 2 ^{o}C/min for 2 h to completely remove the left impurities, at 1400^{o}C with 5 ^{o}C/min for 2 h to crystallization, and cooled down with cooling rate of 10 ^{o}C/min to room temperature. Finally, the obtained materials were ground into ceramic powders using a mortar. Pellets with diameters of 20 mm and 5 mm, were separately compressed under fixed pressure (~130 MPa for 20 mm and ~32 MPa for 5 mm) by a Pellet Press (Specac) and sintered at 1400^{o}C for 10 h, at a heating rate of 10 ^{o}C/min and cooling rate of 15 ^{o}C/min.

2.2 Characterizations

X-Ray Diffraction (XRD) (Bruker D8 Advance) using *Cu K*-alpha radiation as X-Ray source was used to analyse the crystalline phase at room temperature, with scanning range of 2-theta (2θ) from 20^o to 90^o and 85^o to 150^o, and a scanning step of 0.01^o. The voltage and current were 40 KV and 35 mA, respectively. The XRD results were analysed by Eva software. Rietveld refinement was applied to calculate the lattice constants of YAG and doped YAG by using the third Chu-Wan profile (CW profile) function of General Structure Analysis System (GSAS) software [20]. The calculative XRD database was referenced from yttrium aluminium garnet powder obtained from sol-gel method [21].

Thermal Conductivity Analyser (TCA, C-THERM Tci^{TM}) was used to detect thermal conductivities of ceramic pellets with ~20 mm in diameter and a minimum thickness of 3 mm at room temperature. Wakefield solution of T120 silicone was applied between the ceramic pellet and a sensor as thermal joint compound for good contact. The average thermal conductivity was obtained from 10 measurements, and the average values were used in this study. The thermal conductivities of all pellets were corrected from the measured thermal conductivities and their porosities by equation (1) [12]:

$$\frac{k}{k_o} = 1 - \frac{4}{3}\emptyset \qquad (1)$$

where k was the value of measured thermal conductivity using TCA equipment; k_o was the corrected value of sample and $\emptyset$ was the estimated fractional porosity of specimen.

The porosities of pellets were obtained from the relative density calculated by equation (2). The measured density (ρ) of each pellet was calculated by the weight and the volume. The theory density (ρ_{th}) of each pellet was calculated using equation (3) [12]. The volume of unit

cell was calculated from lattice parameters as obtained from XRD results.

$$\emptyset = 1 - \frac{\rho}{\rho_{th}} \qquad (2)$$

$$\rho_{th} = \frac{(MW)(n)}{V_{cell}N_A} \times 10^{27} \qquad (3)$$

where MW is molecular weight; n is formula unit per unit cell; V_{cell} is volume of the unit cell; N_A is Avogadro constant, 6.022×10^{23}. All thermal conductivities discussed in this work are the values after correction.

Thermal Mechanical Analysis (TMA) Q400 was used to measure the CTEs of the ceramic pellets. The diameters of all ceramic pellets were ~5 mm and the applied force was 0.02 N with preload of 0.05 N. The measurement was carried out in nitrogen atmosphere with a flow rate of 50 mL/min from room temperature to 950^{o}C.

The surface microstructure of the ceramic pellets was observed using a FEG XL30 ESEM scanning electron microscope (SEM) with an accelerating voltage of 15 kV. The as-prepared samples were carbon coated prior to SEM observation, and the grain sizes were obtained using software ImageJ.

3 Results and Discussion

3.1 Phase Analysis

The XRD patterns of un-doped and doped YAG powders are presented in Figure 9. **Figure 9 (a)** demonstrates that no extra phase is observed and all materials exhibit single cubic phase with space group Ia3d [21]. The peak shift is much easier to be observed at high 2θ for small amount of Yb doped YAG, as shown in **Figure 9 (b):** peak (11,6,3) and (10,8,2) shift to higher 2θ from A1 to A3, when doping concentration *x* increases from 0.05 to 0.2 in $(Yb_xY_{1-x})_3Al_2Al_3O_{12}$ solid solution, which indicates that Yb^{3+} ions locate on the dodecahedral site and cause shrinkage of the crystal structure, due to the replacement of Y^{3+} ions in dodecahedron with relatively smaller Yb^{3+} ions. On the contrary, peaks (11,6,3) and (10,8,2) slightly shift to lower 2θ from B1 to B3 when doping concentration *x* increases from 0.005 to 0.02 in $Y_3(Yb_xAl_{1-x})_2Al_3O_{12}$ solid solution. Therefore, it is confirmed that Yb^{3+} ions are doped on the octahedral site which resulted from the expansion of the crystal structure, due to the replacement of Al^{3+} ions in octahedron with the relatively larger Yb^{3+} ions. .

In **Figure 10**, the calculated results are well fitted with experimental XRD patterns after the Rietveld Refinement, and the obtained lattice constant is shown in **Figure 11**. As YAG has the cubic phase, *a* equals to *b* and *c*. The lattice constant of un-doped YAG is 12.0116 Å in this work, which is slightly larger than the value (12.0089 Å) reported by Carda *et al* (JCPDS 33–40) [21]. If the Yb^{3+} ions occupy sites in dodecahedron, due to the slightly small ionic radius compared with Y^{3+} ions, distortion would occur in the dodecahedrons, and generate shrinkage in order to achieve stabilized crystal structure. The lattice constant *a* decreases from 12.0088 to 11.9968 Å with the increased doping concentration, which further confirms that Yb^{3+} ions enter dodecahedral site $(Yb_xY_{1-x})_3Al_2Al_3O_{12}$ solid solution. Conversely, crystal

structure expands when the dopant is located on octahedral site due to its relatively large radius, and *a* increases from 12.0164 to 12.0220 Å, which also proves that Yb^{3+} ions are doped in octahedral sites for $Y_3(Yb_xAl_{1-x})_2Al_3O_{12}$ solid solution.

For specimen B2 with 1.5 mol% doping concentration on octahedral site, its lattice constant slightly increases compared with the specimen with 0.5 mol% doping concentration. The result indicates that, a very small amount of Yb^{3+} ions may enter dodecahedral sites then cause the shrinkage of crystal structure, which can weaken the increase of lattice constant.

3.2 SEM images

The grain sizes of doped YAG pellets are investigated from their SEM images as shown in **Figure 12**. The grain sizes in all studied pellets are in the range of 100 nm to 600 nm. The calculated porosities from equation (2) are around 35%, and pores have been observed in each material. The recrystallizations (marked as the red circled regions) also occur in these materials, which would result from the diffusion of ions. Additionally, more recrystallization regions appear in the specimens with higher doping concentrations either on dodecahedral or octahedral sites.

3.3 Thermal conductivity

The thermal conductivities and theoretical densities of doped and un-doped YAG are shown in **Figure 13**. The theoretical density of un-doped YAG (4.55 $g \cdot cm^{-3}$) is very close to the reported data (4.56~4.57 $g \cdot cm^{-3}$) [11, 22]. Furthermore, the theoretical density of doped YAG increases with the increasing doping concentration of Yb^{3+} ions which have the relatively heavy atomic mass compared with Y^{3+} ions. In addition, the thermal conductivity of un-doped YAG is 3.28 $W \cdot m \cdot K^{-1}$ at room temperature, similar to the value reported by Padture (3.2 $W \cdot m \cdot K^{-1}$) [10] and it is relatively high for thermal barrier application. When the doping

concentration of Yb^{3+} ion in dodecahedron is in the range of 5 mol% to 20 mol%, the thermal conductivity decreases from 2.31 $W \cdot m \cdot K^{-1}$ to 2.09 $W \cdot m \cdot K^{-1}$, which is much lower than un-doped YAG. Furthermore, the thermal conductivity is reduced from 2.38 $W \cdot m \cdot K^{-1}$to 2.11 $W \cdot m \cdot K^{-1}$, when doping concentration increases from 0.5 mol% to 2 mol% in octahedron. It is suggested that the thermal conductivity is efficiently reduced by introducing Yb^{3+} ions in octahedron rather than in dodecahedron.

In a dodecahedral site, one Y atom is surrounded by 8 oxygen atoms, so the ionic radius of Y^{3+} is 1.019 Å [16]; while the radius of Yb^{3+} ion with 8 coordination is 0.985 Å [16], which is slightly smaller than that of the host Y^{3+} ion. Because Yb^{3+} ion is relatively smaller in the centre of dodecahedron, it could lead the distortion of dodecahedron for the structural stabilization. Nevertheless, this radial difference between Yb^{3+} and Y^{3+} ions is only 0.034 Å, thus the distortion is indistinctive and do not have strong influence on the structures of neighboured dodecahedron and octahedron. Therefore, the thermal conductivity only decreases slightly and also the doping concentration in dodecahedron is much higher than that doped on octahedral site. However on octahedral site, the radial difference between Yb^{3+} and Al^{3+} ions is 0.333 Å, which is much larger compared with the difference (0.034 Å) between Yb^{3+} and Y^{3+} ions. The large size difference causes the octahedron to expand significantly due to the relatively larger radius of Yb^{3+} ions. Moreover, this expansion can also compress the adjacent dodecahedron structure. Therefore, it is found that doping Yb^{3+} ions in octahedron can effectively reduce thermal conductivity than those in dodecahedron.

3.4 Coefficients of thermal expansion

The coefficients of thermal expansions of un-doped and doped YAGs are plotted in **Figure 14**. It is observed that the dopant does not have a significant effect on thermal expansion

below 300^{o}C whether it is in dodecahedron or octahedron. In **Figure 14 (a)**, the coefficient of thermal expansions of un-doped YAG is 7~10×10^{-6} K^{-1} from 100^{o}C to 950^{o}C and the CTE at low temperature is very similar to the value reported by Klein (~8×10^{-6} K^{-1}) [11]. When introducing relatively smaller Yb^{3+} ions in dodecahedrons, the structure can generate distortion and slightly shrink simultaneously, which creates variation of the interatomic spacing and has a negative effect on thermal expansion of YAG. When the doping concentration is 5 mol%, the values of CTEs are dramatically reduced to ~8.5×10^{-6} K^{-1} at high temperature. With the increasing doping concentration, CTEs increase and become comparative to that of un-doped YAG. Additionally, it is also observed that the CTEs increase much quickly below 300^{o}C, whereas they change very slowly from 300 to 950^{o}C.

Figure 14 (b) gives the CTEs of Yb^{3+} doped on octahedral site, which increase with the increase of the Yb^{3+} doping concentration. When the doping concentrations are 0.5 mol% and 1.5 mol%, the CTE shows slightly lower values than that of un-doped YAG at high temperature. The CTEs of specimen B2 only slightly increase compared with specimen B1, which could result from some Yb^{3+} ions occupying different sites or interstitial space.

When the doping concentration increases to 2.0 mol%, CTEs of ceramic B3 are over 10×10^{-6} K^{-1} at temperature above 800^{o}C, which is higher than that of un-doped YAG. And also, the doping concentration in octahedron is much lower than that in dodecahedron, but the dopants in octahedral sites have significant effect on increasing coefficient of thermal expansion.

Therefore, Yb^{3+} ions as dopant in octahedron can effectively reduce thermal conductivity and also increase the coefficient of thermal expansion, rather than in dodecahedron. Similarly in future work, if doping in dodecahedral site, it is suggested to select a dopant with ionic radius larger than host Y^{3+} ion to effectively reduce thermal conductivity and increase the

coefficient of thermal expansion of YAG.

4 Conclusions

As having the smallest radius in the lanthanide series, Yb^{3+} ions are introduced into dodecahedrons or octahedrons in YAG, and distortion could be generated in the crystal structure that affects the thermal properties. The shifts of XRD peaks and changes of lattice constant indicate that dopants are occupying dodecahedral or octahedral sites, except for ceramic B2, in which some Yb^{3+} ions may occupy different sites or interstitial space. In addition, the thermal conductivity at room temperature can be reduced with the dopant on either site, though the reduction is much more remarkable when the dopant is on octahedral site. The decrease of CTE is observed when doping on dodecahedral site, due to the small radius of Yb^{3+} ions causing the contraction of dodecahedrons. However, coefficient of thermal expansion increases when the dopant occupies a site in octahedron. And the CTE value is over 10×10^{-6} K^{-1} above 800^{o}C, with doping concentration at 2 mol%. Therefore, it is found that Yb^{3+} ions doped on octahedral sites can efficiently reduce thermal conductivity and increase the coefficient of thermal expansion, which is mainly attributed to the larger ionic radial size of Yb^{3+} and the larger radial difference between Yb^{3+} and Al^{3+} ions. In future work, it is suggested that a dopant with larger radius occupy either dodecahedral or octahedral sites to further reduce thermal conductivity and increase coefficient of thermal expansion for YAG as thermal barrier coating material.

Acknowledgement

Jing Wang wishes to acknowledge the studentship support from the University of Nottingham and ACAE.

References:

[1] R.A. Miller, C.E. Lowell. Failure mechanisms of thermal barrier coatings exposed to elevated temperatures, Thin Solid Films 95 (1982) 265-273.

[2] S.K.L. R.J. Bratton. Zirconia thermal barrier coatings, The American Ceramic Society, Columbus, OH, 1981.

[3] S. Meier, D. Gupta, K. Sheffler. Ceramic thermal barrier coatings for commercial gas turbine engines, JOM 43 (1991) 50-53.

[4] Y. Oishi, K. Ando. Oxygen self-diffusion in cubic ZrO_2 solid solutions. in: Simkovich G, Stubican V, (Eds.). Transport in Nonstoichiometric Compounds, vol. 129. Springer US, 1985. pp. 189-202.

[5] J.S. Abell, I.R. Harris, B. Cockayne, B. Lent. An investigation of phase stability in the Y_2O_3-Al_2O_3 system, J. Mater. Sci. 9 (1974) 527-537.

[6] Y.J. Su, R.W. Trice, K.T. Faber, H. Wang, W.D. Porter. Thermal conductivity, phase stability, and oxidation resistance of $Y_3Al_5O_{12}$ (YAG)/Y_2O_3–ZrO_2 (YSZ) thermal-barrier coatings, Oxidation of Metals 61 (2004) 253-271.

[7] L.J. Gu, S.M. Zhao, H.Y. Xu, Y. Hui, X.Z. Fan, B.L. Zou, Y. Wang, X.Q. Cao. Phase stability of plasma sprayed YAG-YSZ composite beads/coatings at high temperature, J. Eur. Ceram. Soc. 33 (2013) 3325-3333.

[8] T.A. Parthasarathy, T.-I. Mah, K. Keller. Creep mechanism of polycrystalline yttrium aluminum garnet, J. Am. Ceram. Soc. 75 (1992) 1756-1759.

[9] J. French. High-temperature deformation and fracture toughness of duplex ceramic microstructures. Ph. D. Thesis. Lehigh Univ., Bethlehem, PA (United States), 1993.

[10] N.P. Padture, P.G. Klemens. Low thermal conductivity in garnets, J. Am. Ceram. Soc. 80 (1997) 1018-1020.

[11] P.H. Klein, W.J. Croft. Thermal conductivity, diffusivity, and expansion of Y_2O_3, $Y_3Al_5O_{12}$, and LaF_3 in the range 77°–300°K, J. Appl. Phys. 38 (1967) 1603-1607.

[12] J. Wang, F. Xu, R.J. Wheatley, K.-L. Choy, N. Neate, X. Hou. Investigation of La^{3+} doped $Yb_2Sn_2O_7$ as new thermal barrier materials, Mater. Des. 85 (2015) 423-430.

[13] C. Ren, Y.D. He, D.R. Wang. Cyclic oxidation behavior and thermal barrier effect of YSZ–(Al_2O_3/YAG) double-layer TBCs prepared by the composite sol–gel method, Surf. Coat. Technol. 206 (2011) 1461-1468.

[14] Y.J. Su, R.W. Trice, K.T. Faber, H. Wang, W.D. Porter. Thermal conductivity, phase stability, and oxidation resistance of $Y_3Al_5O_{12}$ (YAG)/Y_2O_3-ZrO_2 (YSZ) thermal-barrier coatings, Oxidation of Metals 61 (2004) 253-271.

[15] Y.G. Liu, P. Peng, M. Fang, Z. Huang. $Y_{3-x}Er_xAl_5O_{12}$ aluminate ceramics: preparation, thermal properties and theoretical model of thermal conductivity, Adv. Eng. Mater. 14 (2012) 170-177.

[16] D. Lybye, M. Mogensen. Effect of transition metal ions on the conductivity and stability of

stabilised zirconia. Advances in Solid Oxide Fuel Cells II: Ceramic Engineering and Science Proceedings. John Wiley & Sons, Inc., 2008. pp. 67-78.

[17] N.B.I. Ftema W. Aldbea. An overview about the garnet thin films (terbium yttrium iron garnet and aluminum terbium yttrium iron garnet) structural and magnetic properties, Journal of Materials Sciences and Applications 1 (2015) 185-194.

[18] R. Shannon. Revised effective ionic radii and systematic studies of interatomic distances in halides and chalcogenides, Acta Crystallogr., Sect. A: Found. Crystallogr. 32 (1976) 751-767.

[19] I. College. Database of Ionic Radii. the Atomistic Simulation Group in the Materials Department of Imperial College.

[20] L.W. Finger, D.E. Cox, A.P. Jephcoat. A correction for powder diffraction peak asymmetry due to axial divergence, J. Appl. Crystallogr. 27 (1994) 892-900.

[21] J. Carda, M.A. Tena, G. Monros, V. Esteve, M.M. Reventos, J.M. Amigo. A rietveld study of the cation substitution between uvarovite and yttrium-aluminum synthetic garnets, obtained by sol-gel method, Cryst. Res. Technol. 29 (1994) 387-391.

[22] R. Boulesteix, A. Maître, J.F. Baumard, C. Sallé, Y. Rabinovitch. Mechanism of the liquid-phase sintering for Nd:YAG ceramics, Opt. Mater. 31 (2009) 711-715.

List of figure captions

Figure 1: **(a)** The crystal structure of Yttrium aluminium garnet, in which there are three polyhedrons: dodecahedron, octahedron and tetrahedron; **(b)** one octahedron sharing its three edges with three different shared-edge dodecahedrons.

Figure 2: XRD patterns of Yb^{3+} ions doped on dodecahedral and octahedral sites in YAG and un-doped YAG powders **(a)** 2θ from 20 to 90°; **(b)** 2θ from 110 to 115°.

Figure 3: Comparison between the calculative simulation results and the experimental XRD data for the refining unit cell of ceramics **(a)** A1, **(b)** A2, **(c)** A3, **(d)** B1, **(e)** B2 and **(f)** B3, where Diff refers to the difference between the calculative (Calc) and observed (Obs) data.

Figure 4: The change of lattice constant with Yb^{3+} doping concentration in YAG.

Figure 5: SEM images of the pellet surface: (a) $(Yb_{0.05}Y_{0.95})_3Al_2Al_3O_{12}$, A1; (b) $(Yb_{0.15}Y_{0.85})_3Al_2Al_3O_{12}$, A2; (c) $(Yb_{0.2}Y_{0.8})_3Al_2Al_3O_{12}$, A3; (d) $Y_3(Yb_{0.005}Al_{0.095})_2Al_3O_{12}$, B1; (e) $Y_3(Yb_{0.015}Al_{0.085})_2Al_3O_{12}$, B2; and (f) $Y_3(Yb_{0.02}Al_{0.08})_2Al_3O_{12}$, B3. Where the red circles regions present the recrystallization

Figure 6: Thermal conductivities and theoretical densities of Yb^{3+} ions doped YAG in dodecahedron or octahedron and un-doped YAG at room temperature.

Figure 7: **(a)** The CTEs of A1, A2, A3 and YAG from 100°C to 950°C; **(b)** The CTEs of B1, B2 and B3 from 100°C to 950°C.

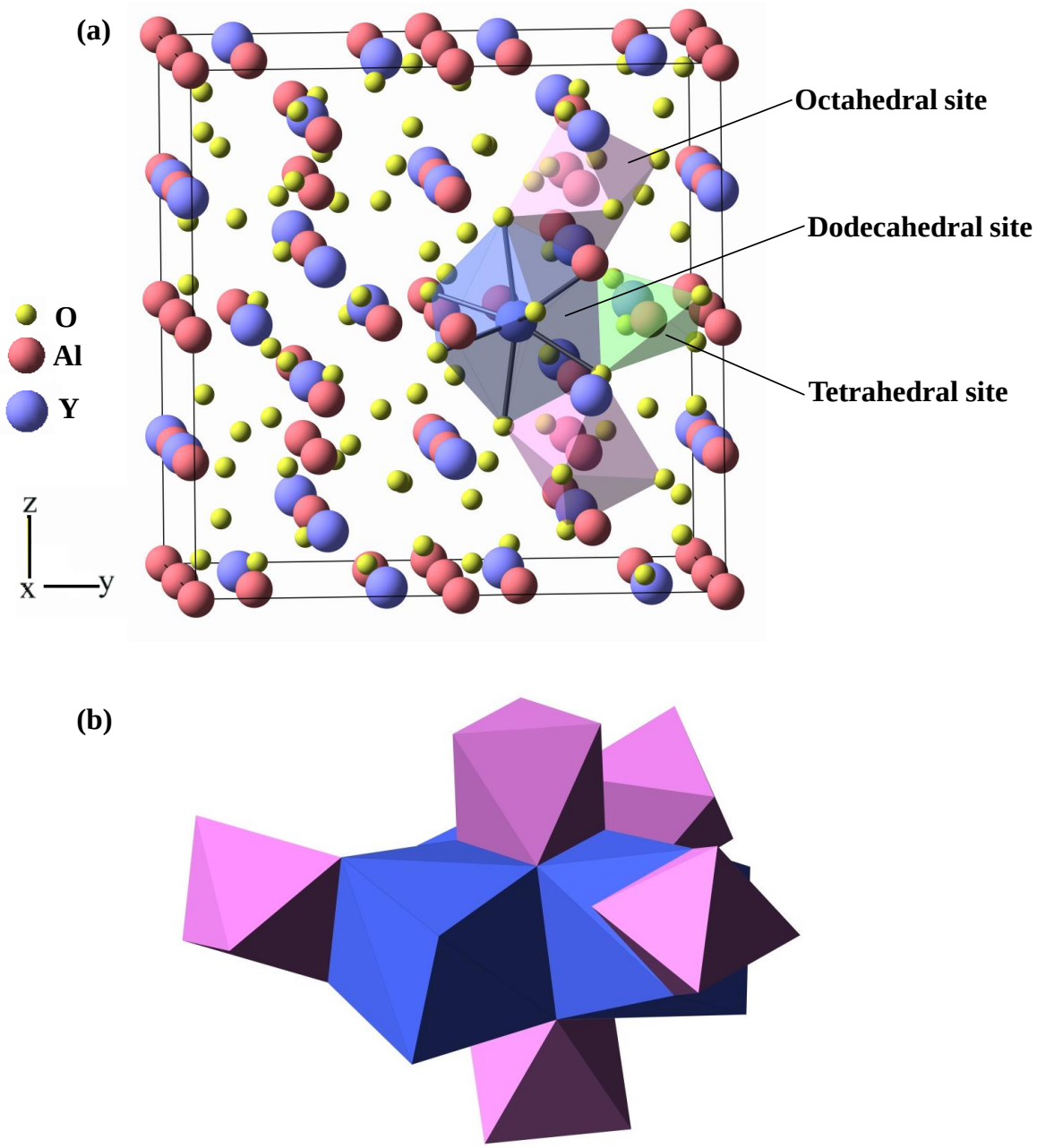

Figure 8: **(a)** The crystal structure of Yttrium aluminium garnet, in which there are three polyhedrons: dodecahedron, octahedron and tetrahedron; **(b)** one octahedron sharing its three edges with three different shared-edge dodecahedrons.

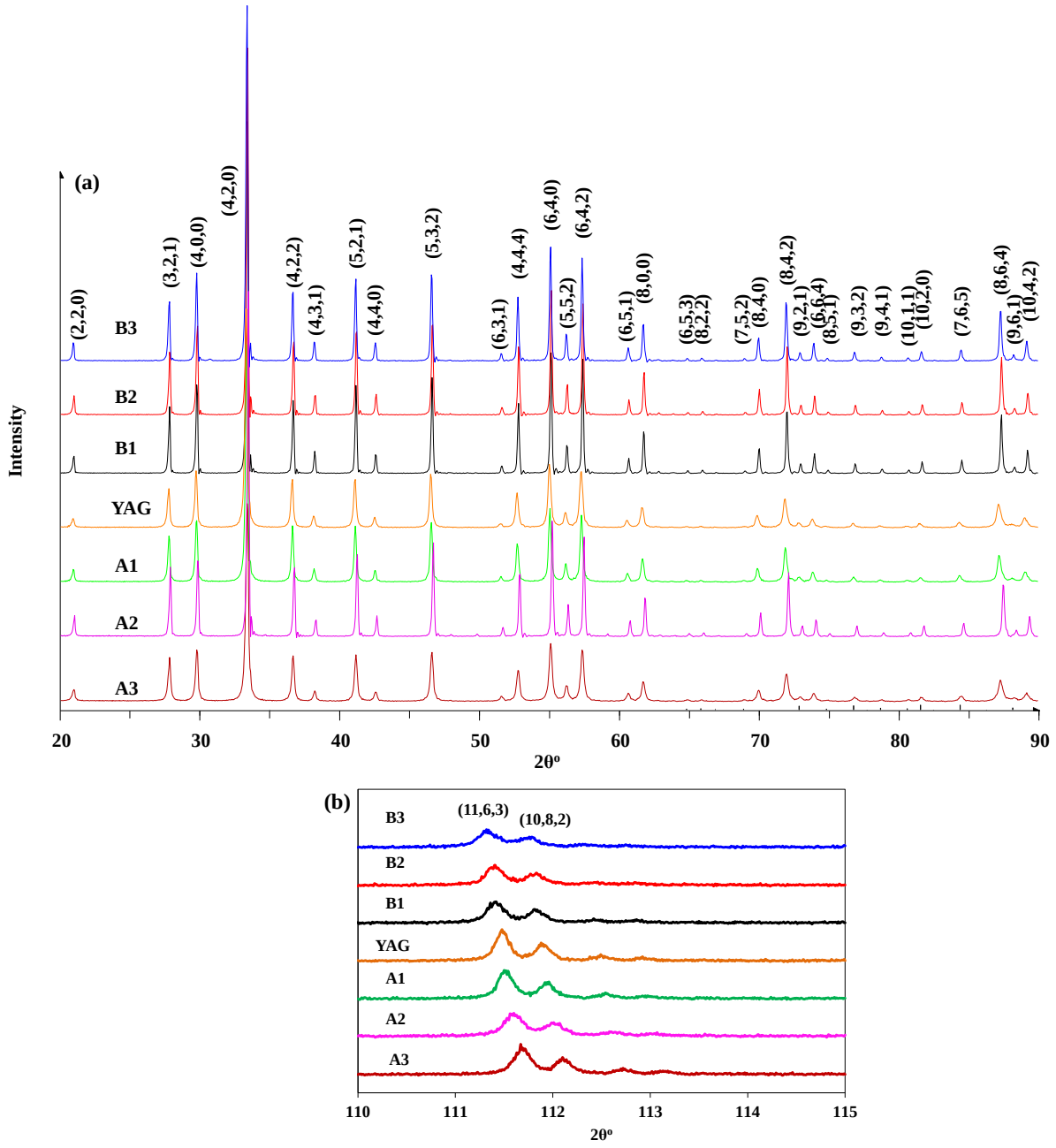

Figure 9: XRD patterns of Yb^{3+} ions doped on dodecahedral and octahedral sites in YAG and un-doped YAG powders **(a)** 2θ from 20 to 90º; **(b)** 2θ from 110 to 115º.

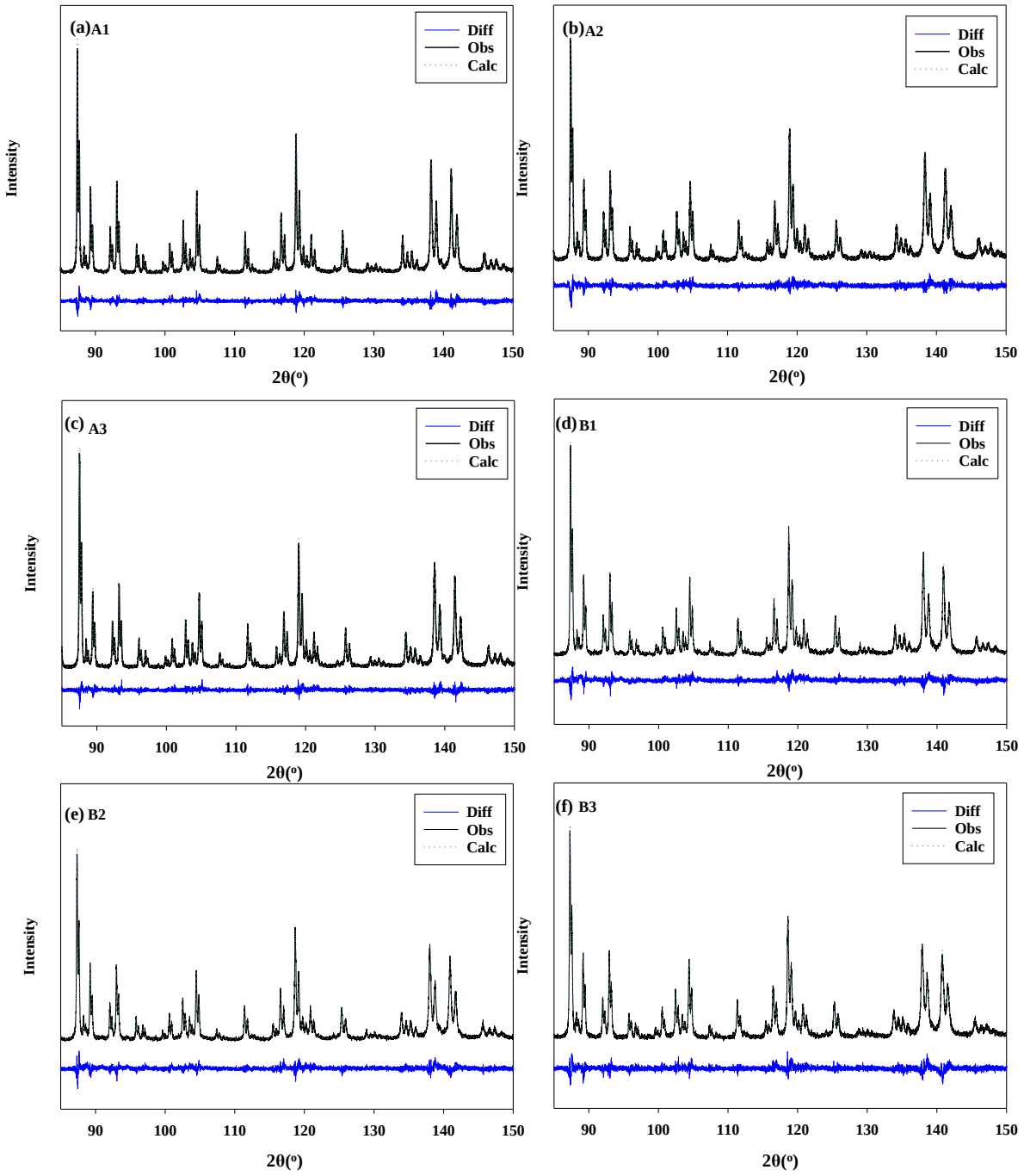

Figure 10: Comparison between the calculative simulation results and the experimental XRD data for the refining unit cell of ceramics **(a)** A1, **(b)** A2, **(c)** A3, **(d)** B1, **(e)** B2 and **(f)** B3, where Diff refers to the difference between the calculative (Calc) and observed (Obs) data.

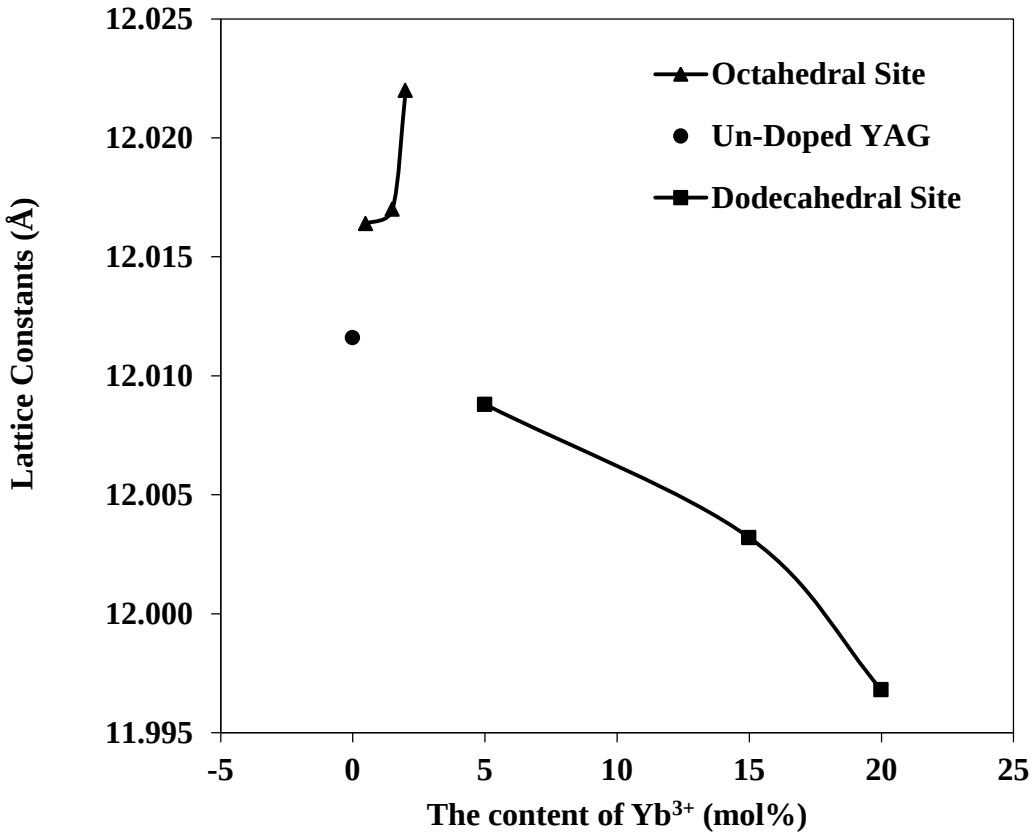

Figure 11: The change of lattice constant with Yb^{3+} doping concentration in YAG.

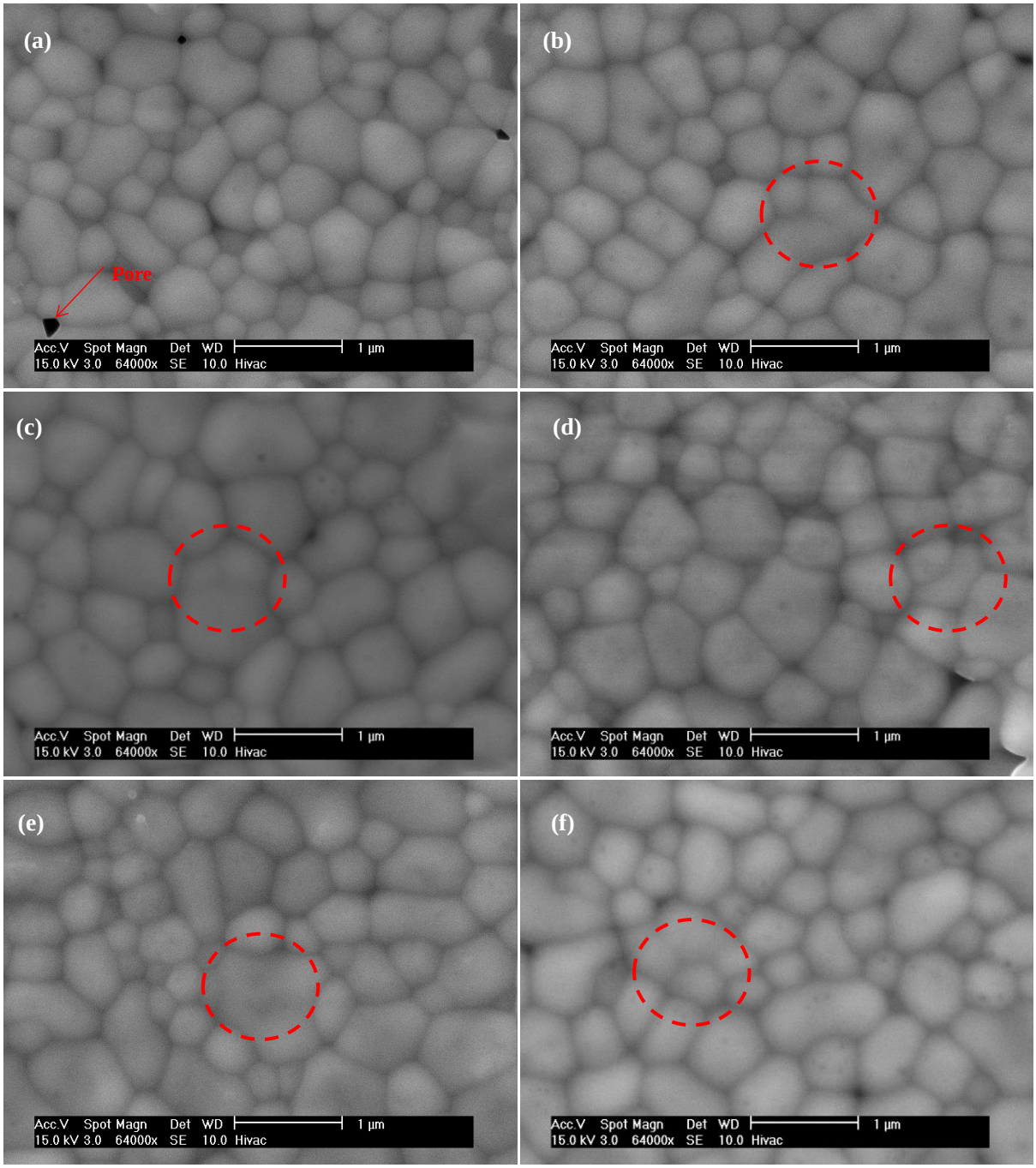

Figure 12: SEM images of the pellet surface: (a) $(Yb_{0.05}Y_{0.95})_3Al_2Al_3O_{12}$, A1; (b) $(Yb_{0.15}Y_{0.85})_3Al_2Al_3O_{12}$, A2; (c) $(Yb_{0.2}Y_{0.8})_3Al_2Al_3O_{12}$, A3; (d) $Y_3(Yb_{0.005}Al_{0.095})_2Al_3O_{12}$, B1; (e) $Y_3(Yb_{0.015}Al_{0.085})_2Al_3O_{12}$, B2; and (f) $Y_3(Yb_{0.02}Al_{0.08})_2Al_3O_{12}$, B3. Where the red circles regions present the recrystallization

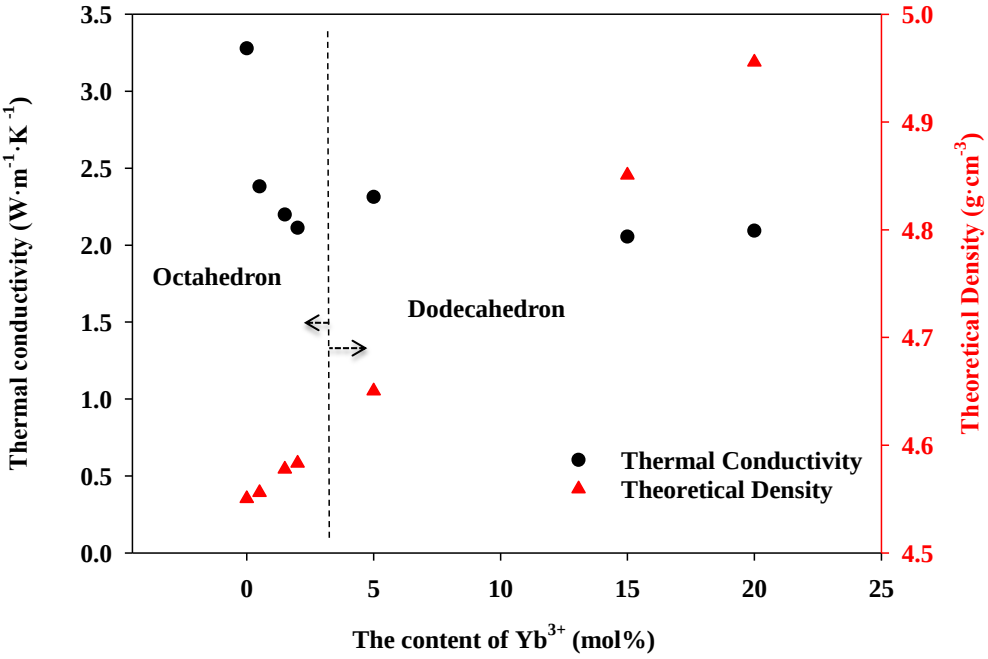

Figure 13: Thermal conductivities and theoretical densities of Yb^{3+} ions doped YAG in dodecahedron or octahedron and un-doped YAG at room temperature.

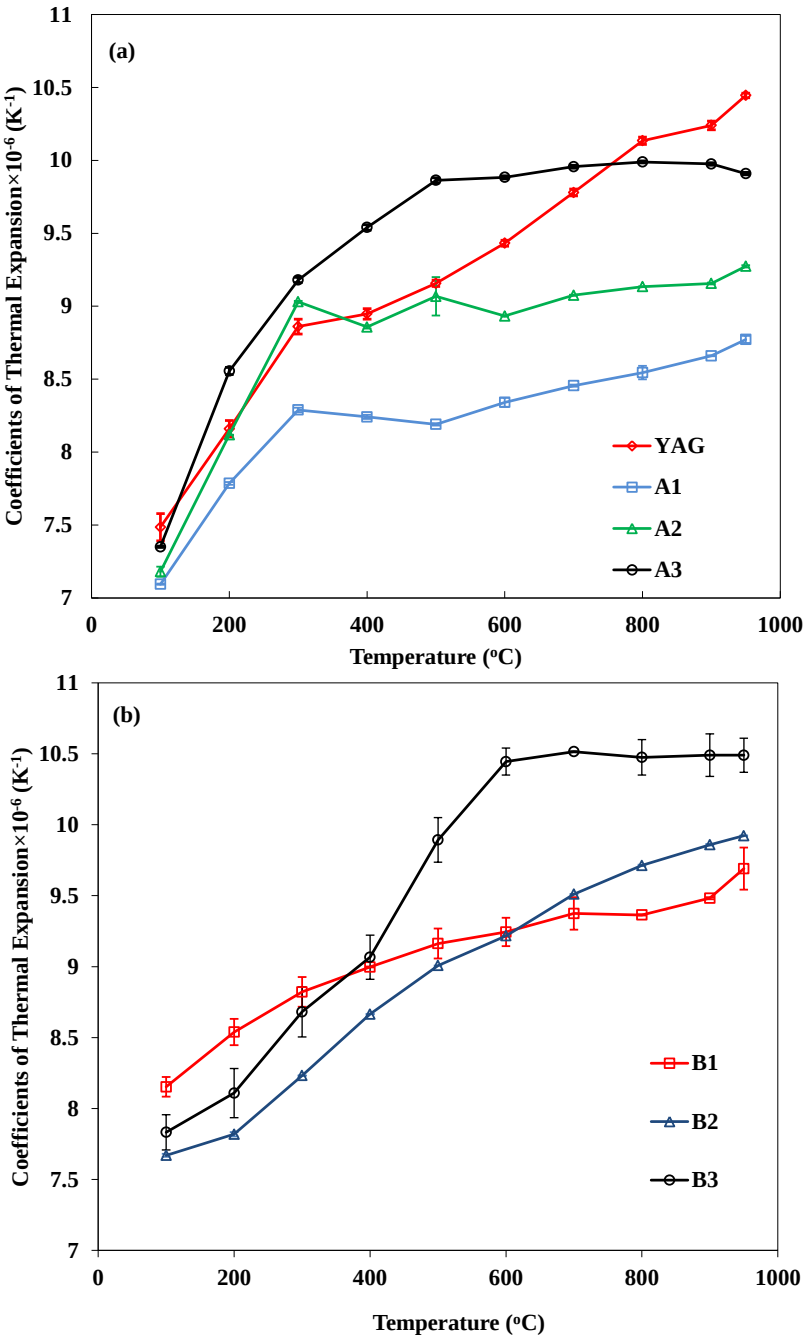

Figure 14: **(a)** The CTEs of A1, A2, A3 and YAG from 100°C to 950°C; **(b)** The CTEs of B1, B2 and B3 from 100°C to 950°C.

Table 1: The stoichiometry of chemical elements in different compositions.

Stoichiometric composition	Chemical element [mole ratio: Y/Al(1)/Al(2)/Yb]			
	Y	Al(1) (in octahedron)	Al(2) (in tetrahedron	Yb
$Y_3Al_2Al_3O_{12}$ (YAG)	3	2	3	0
$(Yb_{0.05}Y_{0.95})_3Al_2Al_3O_{12}$ (A1)	2.85	2	3	0.15
$(Yb_{0.15}Y_{0.85})_3Al_2Al_3O_{12}$ (A2)	2.55	2	3	0.45
$(Yb_{0.20}Y_{0.80})_3Al_2Al_3O_{12}$ (A3)	2.40	2	3	0.60
$Y_3(Yb_{0.005}Al_{0.995})_2Al_3O_{12}$ (B1)	3	1.99	3	0.01
$Y_3(Yb_{0.015}Al_{0.985})_2Al_3O_{12}$ (B2)	3	1.97	3	0.03
$Y_3(Yb_{0.020}Al_{0.980})_2Al_3O_{12}$ (B3)	3	1.96	3	0.04